ChemComm

COMMUNICATION



Cite this: *Chem. Commun.*, 2021, 57, 6899

Received 24th March 2021,
Accepted 12th June 2021

DOI: 10.1039/d1cc01599k

rsc.li/chemcomm

# Magnetic-field-assisted deposition of self-assembling crystallite layers of $Co^{2+}$-containing layered double hydroxides†

Daniel E. L. Vieira, [a] João P. V. Cardoso, [a] Alexey V. Fedorchenko, [b] Elena L. Fertman, [b] Erik Čižmár, [c] Alexander Feher, [c] Roman Yu. Babkin, [d] Yurii G. Pashkevich, *[d] Christopher M. A. Brett, [e] Joaquim M. Vieira [a] and Andrei N. Salak *[a]

**Precipitation of nanocrystallites of cobalt–aluminium layered double hydroxides in a magnetic field has been studied. In a magnetic field perpendicular to the substrate, dense and homogeneous films have been obtained. Magnetic anisotropy of the crystallites is explained by deviation from the statistical cation distribution in favour of honeycomb-like coordination of cobalt.**

The requirement of miniaturization has given rise to the extensive development and study of nanostructures formed using self-assembly or direct assembly of submicron-size objects.[1–4] New functional materials with promising physical and chemical properties have been created.[5,6] It is important that a decrease in dimensionality can result in new features, which do not appear in bulk forms. These effects can be further enhanced by means of formation of arranged 1-D and 2-D nanostructures in external fields.[7,8] Among the first successful examples, application of an external magnetic field during layer-by-layer deposition (LbL) of magnetic FePt nanoparticles was reported.[8] The approach was shown to allow the self-assembly of the nanoparticles in a controlled way and produce ultrathin films with large perpendicular magnetic anisotropy.

Layered double hydroxides (LDH), also known as anion-exchange clays, represent a numerous family of promising 2-D materials with the general formula $[M^{2+}_{1-x}M^{3+}_{x}(OH)_2]^{x+}(A^{y-})_{x/y}\cdot zH_2O$. LDH are composed of alternating positively charged mixed metal $M^{2+}$–$M^{3+}$ hydroxide layers, in which the oxygen octahedral $MO_6$ are edge-linked, and interlayers occupied by anions ($A^{y-}$) and water molecules. The traditional application areas of LDH are catalysis and anion exchange; nevertheless, new functionalities can be generated in these materials using particular $M^{2+}$ and/or $M^{3+}$ cations such as magnetic metal cations[9–15] or luminescent lanthanide ones.[16–18] It should be noticed that in the LDH containing at least one of $Co^{2+}$, $Ni^{2+}$, $Mn^{3+}$, $Cr^{3+}$ or $Fe^{3+}$, the magnetic ordering appears at very low temperatures, which makes direct practical use of the magnetic properties of these materials unlikely. Nevertheless, since the magnetic properties of such LDH are dependent on the cation content and the interlayer distance, they can be used in the development of hybrid magnets and related materials.[19,20]

In 2003, Lukashin *et al.* reported the use of LDH intercalated with anionic complexes containing $Fe^{3+}$ and $Ni^{3+}$ to design anisotropic 2-D magnetic nanocomposites for electronic applications.[21] Eight years later, Shao *et al.* carried out the LbL deposition of Co–Fe LDH in a magnetic field perpendicular to the substrate and obtained continuous and uniform films.[22] However, in their work, no mechanism of the field-assisted film formation was suggested and the magnetic properties of the obtained Co-Fe LDH films were not explored. In 2018, Jose *et al.* observed *in situ* an alignment of monodisperse Mg–Al LDH nanocrystallites into ordered aggregates, suggested a mechanism and specified the conditions of self-assembly of such 2-D LDH nanostructures in wet conditions.[3]

Here we report on the alignment effect of the external magnetic field on the flake-like nano-sized crystallites of cobalt–aluminium LDH in suspensions, which allows formation of dense and homogeneous films. Based on analysis of the magnetic anisotropy of the LDH crystallites, the intrinsic mechanism of the effect has been suggested. Layered double hydroxides with a $Co^{2+}$-to-$Al^{3+}$ molar ratio ($n = (1-x)/x$) of 2 and intercalated with either nitrate or carbonate (hereafter, $Co_2Al$–$NO_3$ and $Co_2Al$–$CO_3$) were the object of this study. In spite of their chemical and structural similarity, these two LDH

[a] *Department of Materials and Ceramic Engineering, CICECO – Aveiro Institute of Materials, University of Aveiro, 3810-193 Aveiro, Portugal. E-mail: salak@ua.pt*
[b] *B. Verkin Institute for Low Temperature Physics and Engineering of the National Academy of Sciences of Ukraine, 61103 Kharkiv, Ukraine*
[c] *Institute of Physics, Faculty of Science, P. J. Šafárik University in Košice, 04154 Košice, Slovakia*
[d] *O. Galkin Donetsk Institute for Physics and Engineering, National Academy of Sciences of Ukraine, 03028 Kyiv, Ukraine. E-mail: yu.pashkevich@gmail.com*
[e] *Department of Chemistry, CEMMPRE, Faculty of Sciences and Technology, University of Coimbra, 3004-535 Coimbra, Portugal*

† Electronic supplementary information (ESI) available: Experimental section, STEM and SEM images, XRD patterns, results of magnetic measurements, and details of the theoretical calculations. See DOI: 10.1039/d1cc01599k

compositions are different in the way their anions are arranged in the interlayers, that results in a considerable difference in the interlayer height values.

$Co_2Al$–$NO_3$ LDH was synthesized using the conventional co-precipitation method.[14] $Co_2Al$–$CO_3$ LDH was obtained *via* nitrate-to carbonate anion exchange at room temperature (Fig. S1, ESI†). To accelerate the crystallization of the parent LDH as well as the anion exchange, high-power sonication was employed during both these stages. The sonication procedure was adapted from our previous work.[23] Crystallites of the obtained LDH were found to be flake-like with a characteristic diameter and thickness of about 400 nm and 20 nm, respectively (Fig. S2, ESI†). Details of the sample preparation procedures as well as of the characterization methods used to monitor their phase content and morphology can be found in the ESI.†

The layers of LDH crystallites were obtained by their natural precipitation from the diluted suspensions in ethanol in zero and non-zero external magnetic field, directed either along or across the precipitation direction (see the ESI† for more detail).

Fig. 1 shows scanning electron microscopy (SEM) images of the obtained LDH layers in both cross-section and top view modes. When the magnetic field is directed vertically (perpendicularly to the substrate surface, Fig. 1a), dense homogeneous films are obtained. The X-ray diffraction (XRD) patterns clearly indicate the preferred orientation of the LDH crystallites in these films (Fig. S3, ESI†). When the magnetic field is horizontal (parallel to the substrate surface) (Fig. 1b) and when there is zero field (Fig. 1c), the obtained layers of the precipitated LDH crystallites are very similar. The thickness of the layers is 3–4 times greater than that of the dense films shown in Fig. 1a, which evidences a porous structure of randomly oriented crystallites in these layers.

The ordered arrangement of the LDH crystallites in the films precipitated in the vertically-directed magnetic field is also evident from the magnetic measurements (Fig. S4 and S5 in the ESI,† respectively). These films demonstrate a considerably higher value of the maximum magnetic moment and more rectangular hysteresis loops than those precipitated in the external field parallel to the substrate surface or in zero field.

The magnetic field apparently arranges the suspended crystallites parallel to each other. The mutual parallel orientation of monodisperse LDH crystallites creates conditions for their self-assembly through the oriented attachment (OA) mechanism.[3] A vertically directed magnetic field causes the suspended flake-like crystallites to align, assemble and precipitate parallel to the substrate surface. In the horizontally-directed field, the flakes can form 2-D aligned structures with the main planes perpendicular to the substrate. However, such structures collapse after impact with the substrate surface or with the previously precipitated crystallites. Therefore, the resulting layer consists of randomly oriented crystallites making it morphologically similar to that obtained in the case of precipitation in a zero field (cf.: Fig. 1b and c).

For $Co_2Al$–$CO_3$ LDH (Fig. S6, ESI†), the microstructure of the layers prepared with different magnetic field directions or in zero field is very similar to that observed with the samples of $Co_2Al$–$NO_3$ LDH.

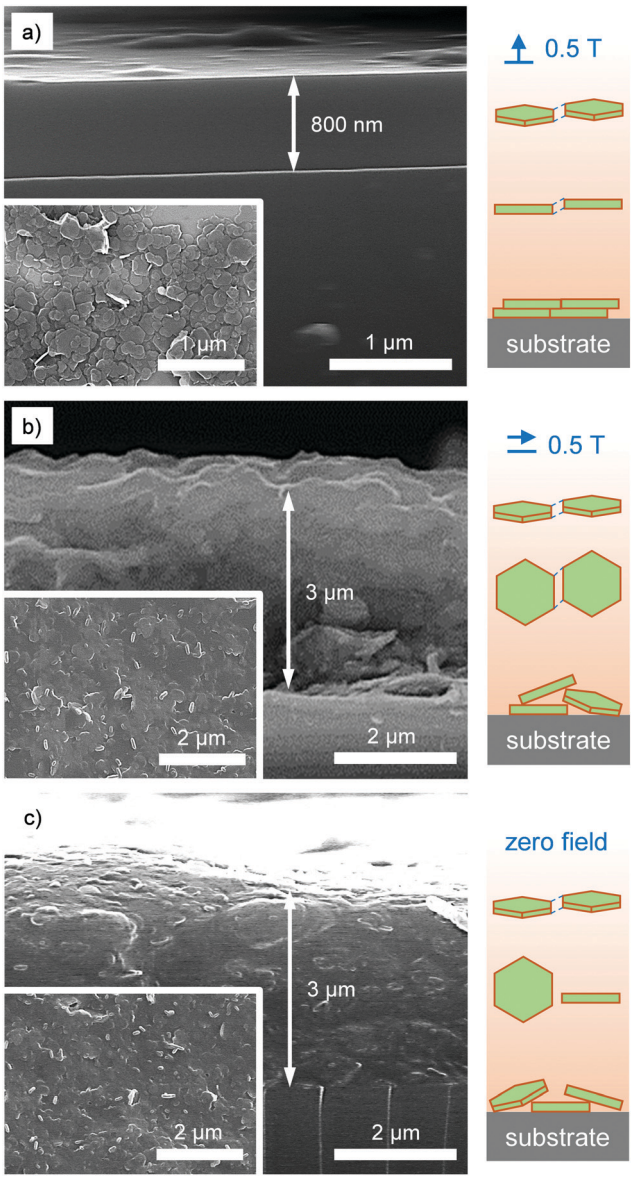


Fig. 1 SEM images (cross section view) of layers of the $Co_2Al$–$NO_3$ LDH crystallites deposited on glass substrates in a magnetic field directed (a) perpendicularly to the substrate surface, (b) parallel to the substrate surface and (c) in a zero magnetic field. Insets show the top views of the respective layers.

It should be recalled that the magnetic order in LDH containing at least one of $Co^{2+}$, $Ni^{2+}$, $Mn^{3+}$ and $Fe^{3+}$ appears at very low temperatures (in particular, an onset of spontaneous magnetisation is detected in $Co_2Al$–$NO_3$ and $Co_2Al$–$CO_3$ at 4.0 K[14] and 4.8 K,[24] respectively). Hence, at room temperature, the magnetic moments of their crystallites are zero and the fact that they are aligned in an external magnetic field is explained by their magnetic anisotropy.

LDH crystallites are naturally anisotropic just because of their layered nature. The perfect LDH crystal is determined by the crystal symmetry to be a flat hexagon prism. Indeed, LDH crystallites with such a shape are usually observed. The diameter-to-thickness ratio of the crystallites depends on the

 

molar relation between the metal cations[25] and in the case of $M^{2+}/M^{3+} = 2$, is typically 20 : 1 (Fig. S2, ESI†). Therefore, it seems reasonable to assume that the magnetic anisotropy of the $Co_2Al$ LDH is caused by structural anisotropy.

The cations in the LDH hydroxide layers form a honeycomb frame. Although a 2 : 1 long-range ordering in the arrangement of cations in the LDH with $M^{2+}/M^{3+} = 2$ appears to be likely and (in the case of considerable cation size difference) favourable, such an ordering is not observed in practice even when their atomic scattering powers are sufficiently different.[26] It should be noted here that long-range cation ordering would be hardly possible to detect using diffraction methods because of high pseudosymmetry, micro-crystallinity and stacking faults,[27] which are very typical of synthetic LDH. The most prominent example of possible ideal order may arise in the $Co_2Al$ LDH where, in the case of undisturbed translation symmetry, every aluminium cation has six $Co^{2+}$ cations as nearest neighbours and every cobalt cation is surrounded by three $Co^{2+}$ and three $Al^{3+}$. In such an ideal case, the net of cobalt cations forms a magnetic honeycomb lattice.

An XRD study of $Co_2Al$–$NO_3$ (Fig. S1, ESI†) revealed no superlattice diffraction reflections, which are anticipated in the case of the 2 : 1 long-range ordering of $Co^{2+}$ and $Al^{3+}$. The structure of this LDH was successfully refined using the space group $R\bar{3}m$[28] in the hexagonal setting with the ***ab***-plane parallel to the hydroxide layers and the ***c***-axis perpendicular to the layer plane. In such a structure model, the atomic sites for cobalt and aluminium are considered the same, that implies a random distribution of these cations in the lattice and equal cation-oxygen bond lengths: $L_{LDH}(Co–O) = L_{LDH}(Al–O) = 2.002$ Å. At the same time, the average distances calculated using Shannon's empirical ionic radii for $Co^{2+}$ (high spin), $Al^{3+}$ and $O^{2-}$ (all six-fold coordinated)[29] for these pairs are $L_{ox}(Co–O) = 2.145$ Å and $L_{ox}(Al–O) = 1.935$ Å. The difference, 0.21 Å, is rather large and suggests that the metal-oxygen octahedra in Co–Al LDH are distorted. The distortions appear to induce magnetic anisotropy in these LDH, since a condition of the ideal oxygen octahedra around cobalt cations results in an isotropic magnetic framework.

It is clear that the distortion of a particular $CoO_6$ octahedron depends on the local environment. There are thirteen possible coordinations of a cobalt cation by neighbouring cations as shown in Fig. 2a. The statistical weights of each coordination for LDH with the Co/Al ratio, $n = 2$, 3 and 4, have previously been found.[15]

In the structural model for theoretical calculations and analysis of magnetic anisotropy, the distances between the nearest cations were considered to be the same (the cation coordinates were taken from the aforementioned structural model, in which the positions of $Co^{2+}$ and $Al^{3+}$ are undistinguishable,[28] and fixed), while oxygens were allowed to shift in order to comply with the bond lengths $L_{ox}(Co–O)$ and $L_{ox}(Al–O)$ indicated above. To meet these conditions, (i) the common oxygen for three neighbouring Co cations shifts by 0.213 Å perpendicular to the ***ab***-plane; (ii) the common oxygen for two Co and one Al neighbouring cations shifts towards the Al ion by 0.158 Å with the displacement vector in the ***ab***-plane;

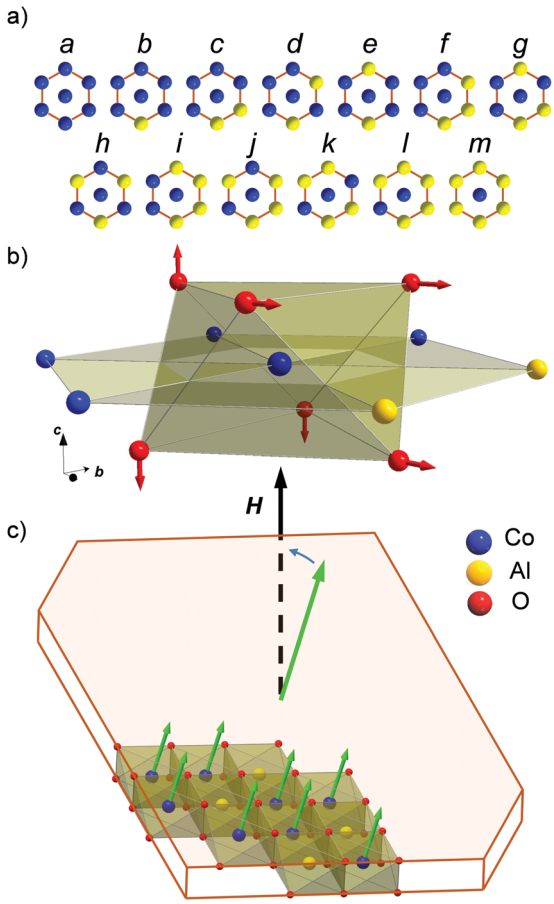


Fig. 2 (a) The thirteen (*a*–*m*) possible cation coordinations of cobalt.[15] (b) Distortion of oxygen octahedron around $Co^{2+}$ with the local environment of the *c*-type: four cobalt ions and two aluminium ions. Hydrogen ions are not shown. (c) Scheme of the action of magnetic field on a hexagonal crystallite of $Co_2Al$ LDH. A fragment of the oxygen octahedral layer is only shown. The green arrows represent magnetic moments $\boldsymbol{m} = g_{zz}\mu_B\boldsymbol{H}$ of $Co^{2+}$ cations. The directional anisotropy arises due to the anisotropy of the magnetic susceptibility, $\chi_{zz} \gg \chi_{xx}$.

(iii) the common oxygen for one Co and two Al neighbouring cations is shifted from the middle of the Al–Al connecting line by 0.158 Å and with the displacement vector in the ***ab***-plane. It is also required that the O–H bonds, $L_{LDH}(O–H) = 0.97$ Å,[28] which are perpendicular to the hydroxide layer,[15] in the cases (ii) and (iii), are tilted by 12° in the direction opposite to the oxygen displacement. An example of the $CoO_6$ octahedron distorted due to the shifted oxygens is shown in Fig. 2a. It is important to emphasize here that in the analysis of the magnetic anisotropy of $Co_2Al$ LDH done in this work, the nature (provided that it is not magnetic) and dimensions of the intercalated anion were not important.

The energy spectra of $Co^{2+}$ (configuration $3d^7$, basic term $^4F$, high spin) for all the thirteen cation coordinations (Fig. 2a) were calculated using the models of the distorted octahedra described above. The Modified Crystal Field Theory[30] was used (see the ESI† for more detail).

In the low temperature range, where magnetic ordering in $Co_2Al$ LDH occurs, only the lowest Kramers doublet in each

configuration is relevant. The respective components, $g_{ij}$ ($i,j$ = $x,y,z$), of the Landé $g$ factor were calculated. The Cartesian coordinate system, where the $x$-axis and the $z$-axis are parallel to the basis vectors $\boldsymbol{a}$ and $\boldsymbol{c}$, respectively, were used. The results of the calculations demonstrate that the values of $g_{xx}$ and $g_{zz}$ of cobalt in $Co_2Al$ LDH depend on the particular cation coordination ($a$–$m$): *cf.* $g_{xx}(c) = 3.65$, $g_{zz}(c) = 1.88$, while $g_{xx}(h) = 0.27$, $g_{zz}(h) = 6.61$. Distribution of the $xx$- and $zz$-components of the g factor among all possible cation coordinations of cobalt in $Co_2Al$ LDH is shown in Fig. S7 (ESI†). The most symmetric cobalt coordination ($h$), which is the basic unit of the ideal Co–Al ordering in $Co_2Al$ LDH, shows the abnormally large $g$ factor anisotropy with $g_{zz} \gg g_{xx}$.

The average values of $g$ factors calculated in this low-temperature approximation using the statistical weight of each of the possible cobalt coordinations (Table S1, ESI†) were found to be only slightly different, and $(g_{zz})_{av}$ is smaller than $(g_{xx})_{av}$. The average values of the $xx$- and $zz$-components of the magnetic susceptibility at room temperature are very similar. In order to calculate the magnetic susceptibility for every configuration, the four lowest Kramers doublets with energies below 300 $cm^{-1}$ are taken into consideration (Table S2, ESI†). Therefore, if cobalt and aluminium are statistically distributed over the thirteen ($a$–$m$) possible local environments, no magnetic anisotropy occurs in the $Co_2Al$ LDH flake-like crystallites.

The magnetic anisotropy of the LDH flakes may arise, if the fully random statistical distribution of cobalt and aluminium is violated and if the weight of some cobalt coordinations prevail sufficiently over the others. Short-range order, which is not detectable in XRD, may induce some preferable cation environment(s). In $Co_2Al$ LDH, a honeycomb-like short-range order forms within the $h$-type coordination. As mentioned above, the $h$-type provides the most pronounced anisotropy of the $g$ factor. Hence, a relatively small disbalance in the random cation distribution in favour of $h$-type will induce magnetic anisotropy of the LDH flakes, with the value of the $zz$-component of the magnetic susceptibility higher than that of the $xx$-component. In such a case, a suspended flake will turn to make the Co–Al hydroxide layer plane perpendicular to the magnetic field direction as shown in Fig. 2c.

In conclusion, we explored the aligning effect of magnetic field to form highly-oriented dense layers of flake-like nanocrystallites of $Co_2Al$–$NO_3$ and $Co_2Al$–$CO_3$LDH with the flake surfaces perpendicular to the direction of the magnetic field. This effect is an indication of the magnetic anisotropy of cobalt cations in the LDH crystallites, which is likely to be induced by the honeycomb-type lattice, which prevails over the statistical distribution of the cation coordinations of $Co^{2+}$.

This work was supported by the bilateral Belarus-Ukraine project T20YKA-020/N0120U000216 (2020–2021). The Slovakia-Portugal project FAST-LDH/APVV-SK-PT-18-0019 (2019–2020). The research done in University of Aveiro was supported by the project CICECO-Aveiro Institute of Materials, UIDB/50011/2020 & UIDP/50011/2020, financed by national funds through the Portuguese Foundation for Science and Technology (FCT)/MCTES. D. E. L. Vieira and J. P. V. Cardoso acknowledge the financial support of FCT-Portugal through the individual PhD grants PD/BD/143033/2018 and SFRH/BD/145281/2019, respectively.

## Conflicts of interest

There are no conflicts to declare.

## Notes and references

1 C. H. Zhou, Z. F. Shen, L. H. Liu and S. M. Liu, *J. Mater. Chem.*, 2011, **21**, 15132.
2 J. Yang, K. Kim, Y. Lee, K. Kim, W. C. Lee and J. Park, *FlatChem*, 2017, **5**, 50.
3 N. A. Jose, H. C. Zeng and A. A. Lapkin, *Nat. Commun.*, 2018, **9**, 4913.
4 S. K. Ghosh and A. Böker, *Macromol. Chem. Phys.*, 2019, **220**, 1900196.
5 D. Deng, K. S. Novoselov, Q. Fu, N. Zheng, Z. Tian and X. Bao, *Nat. Nanotechnol.*, 2016, **11**, 218.
6 G. Fiori, F. Bonaccorso, G. Iannaccone, T. Palacios, D. Neumaier, A. Seabaugh, S. K. Banerjee and L. Colombo, *Nat. Nanotechnol.*, 2014, **9**, 768.
7 J. I. Park, Y. W. Jun, J. S. Choi and J. Cheon, *Chem. Commun.*, 2007, 5001.
8 M. Suda and Y. Einaga, *Angew. Chem., Int. Ed.*, 2009, **48**, 1754.
9 M. Intissar, R. Segni, C. Payen, J. P. Besse and F. Leroux, *J. Solid State Chem.*, 2002, **167**, 508.
10 E. Coronado, J. R. Galan-Mascaros, C. Marti-Gastaldo, A. Ribera, E. Palacios, M. Castro and R. Burriel, *Inorg. Chem.*, 2008, **47**, 9103.
11 J. J. Almansa, E. Coronado, C. Martí-Gastaldo and A. Ribera, *Eur. J. Inorg. Chem.*, 2008, 5642.
12 E. Coronado, C. Martí-Gastaldo, E. Navarro-Moratalla and A. Ribera, *Appl. Clay Sci.*, 2010, **48**, 228.
13 F. Giovannelli, M. Zaghrioui, C. Autret-Lambert, F. Delorme, A. Seron, T. Chartier and B. Pignon, *Mater. Chem. Phys.*, 2012, **137**, 55.
14 D. E. L. Vieira, A. N. Salak, A. V. Fedorchenko, Yu. G. Pashkevich, E. L. Fertman, V. A. Desnenko, R. Yu. Babkin, E. Čižmár, A. Feher, A. B. Lopes and M. G. S. Ferreira, *Low Temp. Phys.*, 2017, **43**, 1214.
15 R. Yu. Babkin, Yu. G. Pashkevich, A. V. Fedorchenko, E. L. Fertman, V. A. Desnenko, A. I. Prokhvatilov, N. N. Galtsov, D. E. L. Vieira and A. N. Salak, *J. Magn. Magn. Mater.*, 2019, **473**, 501.
16 P. Vicente, M. E. Pérez-Bernal, R. J. Ruano-Casero, D. Ananias, F. A. Almeida Paz, J. Rocha and V. Rives, *Microporous Mesoporous Mater.*, 2016, **226**, 209.
17 A. Smalenskaite, D. E. L. Vieira, A. N. Salak, M. G. S. Ferreira, A. Katelnikovas and A. Kareiva, *Appl. Clay Sci.*, 2017, **143**, 175.
18 A. Smalenskaite, A. N. Salak and A. Kareiva, *Mendeleev Commun.*, 2018, **28**, 493.
19 G. Abellán, C. Martí-Gastaldo, A. Ribera and E. Coronado, *Acc. Chem. Res.*, 2015, **48**, 1601.
20 Q. Wang and D. O'Hare, *Chem. Rev.*, 2012, **112**, 4124.
21 A. V. Lukashin, A. A. Vertegel, A. A. Aliseev, M. P. Nikiforov, P. Gornert and Yu. Tretyakov, *J. Nanoparticle Res.*, 2003, **5**, 455.
22 M. Shao, M. Wei, D. G. Evans and X. Duan, *Chem. Commun.*, 2011, **47**, 3171.
23 D. Sokol, D. E. L. Vieira, A. Zarkov, M. G. S. Ferreira, A. Beganskiene, V. V. Rubanik, A. D. Shilin, A. Kareiva and A. N. Salak, *Sci. Rep.*, 2019, **9**, 1.
24 J. A. Carrasco, S. Cardona-Serra, J. M. Clemente-Juan, A. Gaita-Ariño, G. Abellán and E. Coronado, *Inorg. Chem.*, 2018, **57**, 2013.
25 A. N. Salak, A. D. Lisenkov, M. L. Zheludkevich and M. G. S. Ferreira, *ECS Electrochem. Lett.*, 2014, **3**, C9.
26 D. E. Evans and R. C. T. Slade, Structural aspects of layered double hydroxides, in *Structure & Bonding*, Springer-Verlag, Berlin, Germany, 2005, vol. 119, pp. 1–87.
27 W. Hofmeister and H. Von Platen, *Crystallogr. Rev.*, 1992, **3**, 3.
28 A. V. Radha, P. V. Kamath and C. Shivakumara, *Acta Crystallogr., Sect. B: Struct. Sci.*, 2007, **63**, 243.
29 R. D. Shannon, *Acta Crystallogr., Sect. A: Cryst. Phys., Diffr., Theor. Gen. Crystallogr.*, 1976, **32**, 751.
30 K. V. Lamonova, S. M. Orel and Yu. G. Pashkevich, *Modified Crystal Field Theory and its Applications*, Akademperiodyka, Kyiv, 2019, p. 226.

 